J. Fluid Mech. (1995), *vol.* 287, *pp.* 75–92

Another look at unidirectional turbulent flow

By A. J. REYNOLDS[1] AND K. WIEGHARDT[2]

[1] Brunel University, Uxbridge, Middlesex, UB8 3PH, UK

[2] Formerly of Institut für Schiffbau der Universität Hamburg

(Received 23 December 1993 and in revised form 26 September 1994)

Here we consider the mean velocity profile in the core region of a unidirectional turbulent flow, that is, a flow in which the turbulent motion is superposed upon parallel time-averaged streamlines. A kinematical variational principle, originally developed for three-dimensional free-turbulent motions, is shown to be applicable to significant parts of the velocity profiles for flows of both Couette and Poiseuille types. In addition to pure plane Couette and pure plane Poiseuille flows, the motions considered include a variety of admixtures produced by blowing through a wide flat channel one of whose walls comprises a belt which moves either in the direction of the blowing or counter to it.

1. Introduction

Although unidirectional flows are the simplest to describe mathematically, their experimental realization is rather difficult. Test results for a considerable variety of such flows have been given by El Telbany & Reynolds (1980, 1981, 1982). The flows considered were established in a flat channel whose aspect ratio was changed between 12 and 28 (this is the ratio of the channel dimensions in the y- and z-directions) and where one wall is a fixed plate, while the second is a belt which could be moved either in the direction in which air is blown through the channel or in the direction opposite to the blown air. In view of the high aspect ratios adopted, the motion in the central part of the channel can be taken to be approximately independent of the transverse coordinate z. The papers referred to present values of the intensities of the components of turbulence

$$\overline{u'^2}(y), \quad \overline{v'^2}(y), \quad \overline{w'^2}(y)$$

for the x-, y- and z-directions, respectively, as well as the time-mean velocity $U(y)$, where the coordinate y is measured from one of the walls bounding the flow.

Here we are concerned mainly with the specification of the mean velocity $U(y)$ in the core region of this class of flows, that is, the region beyond the wall layers within which the velocity usually varies logarithmically. The actual generation of turbulence in this central region is small compared with that near the wall or the belt, and this suggests that the core flow might be similar in other ways to free-turbulent flow well away from a wall.

2. The variational principle

For a three-dimensional stationary and incompressible flow, in which the local Reynolds number is high enough to justify the neglect of viscous stresses, the equation of motion for the ensemble average velocity field V can be written

$$\frac{\mathrm{D}V}{\mathrm{D}t} = V\cdot\nabla V = \tfrac{1}{2}\nabla V^2 - V\times \mathrm{rot}\, V = -\frac{\nabla p}{\rho} + \frac{T}{\rho} \quad \text{with} \quad \frac{T_i}{\rho} = -\frac{\partial}{\partial x_j}(\overline{u_i' u_j'}),$$

where ρ is the constant density, and T is the volume force associated with the Reynolds stresses. The vorticity equation connecting second derivatives of the mean velocity with those of the Reynolds stresses is

$$-\mathrm{rot}\, L = \mathrm{rot}\, T/\rho, \tag{1}$$

where

$$L = V\times\omega \quad \text{with} \quad \omega = V.$$

Extensive wind-tunnel measurements near the stern of double models of full ships (that is, ships with bluff sterns and a large wake), using laser-Doppler techniques and a grid mesh of 2 or 3 mm, have shown that in three-dimensional free turbulence

$$V \perp \mathrm{rot}\, L \quad \text{or} \quad V\cdot \mathrm{rot}\, L = 0 \tag{2}$$

even in regions with backflow (Wieghardt 1990, 1991; Knaack 1992).

Seeking a quantity for which a variational principle can be set down, we define

$$A = V\times L = (V\cdot\omega)\, V - V^2\omega. \tag{3}$$

The experimentally determined result for three-dimensional flows (that is, equation (2)) implies that $\nabla\cdot A = 0$, since $\nabla\cdot V = 0$. This result is trivial only for flows that are confined to one or two dimensions. However, even in those cases the application of the other basic vector operator, to obtain $\mathrm{rot}\, A$, in general gives a non-zero result.

As a next step, an attempt was made to see whether at least the integral of $(\mathrm{rot}\, A)^2$ becomes a minimum in a region of free turbulence. This leads to a variational principle:

$$I = \iiint (\mathrm{rot}\, A)^2 \,\mathrm{d}x\,\mathrm{d}y\,\mathrm{d}z \to \text{minimum} \tag{4}$$

with the Eulerian equation

$$\mathrm{rot}\,\mathrm{rot}\,\mathrm{rot}\, A = \mathrm{rot}^{\mathrm{III}} A = 0. \tag{5}$$

Since this is a differential equation of the fourth order (for V), numerous solutions for the mean velocity distribution can be obtained. For example, any potential flow with $A = 0$ could be superposed, provided that it complies with the boundary conditions at the edge of the region of free turbulence.

Furthermore, to check the validity of this principle, one has to know the measured velocity field very precisely. A similar situation arose in connection with the law for the outer region of two-dimensional boundary layers. At first the flow was taken to be almost one-dimensional (Wieghardt 1990), provided that the pressure gradient was not too large. Subsequently (Wieghardt 1991), the linear increase of the angle between streamlines and the wall was approximated by a locally radial flow. When this was done, all the boundary layers considered by Coles & Hirst (1968) – even those nearest separation in plane and axial diffusers – were found to be consistent with the Eulerian condition (5).

In the unidirectional flows considered here, A becomes simply U^2U_y. Omitting a factor of 3 for simplicity, we obtain

$$A = (U^3)_y. \tag{6}$$

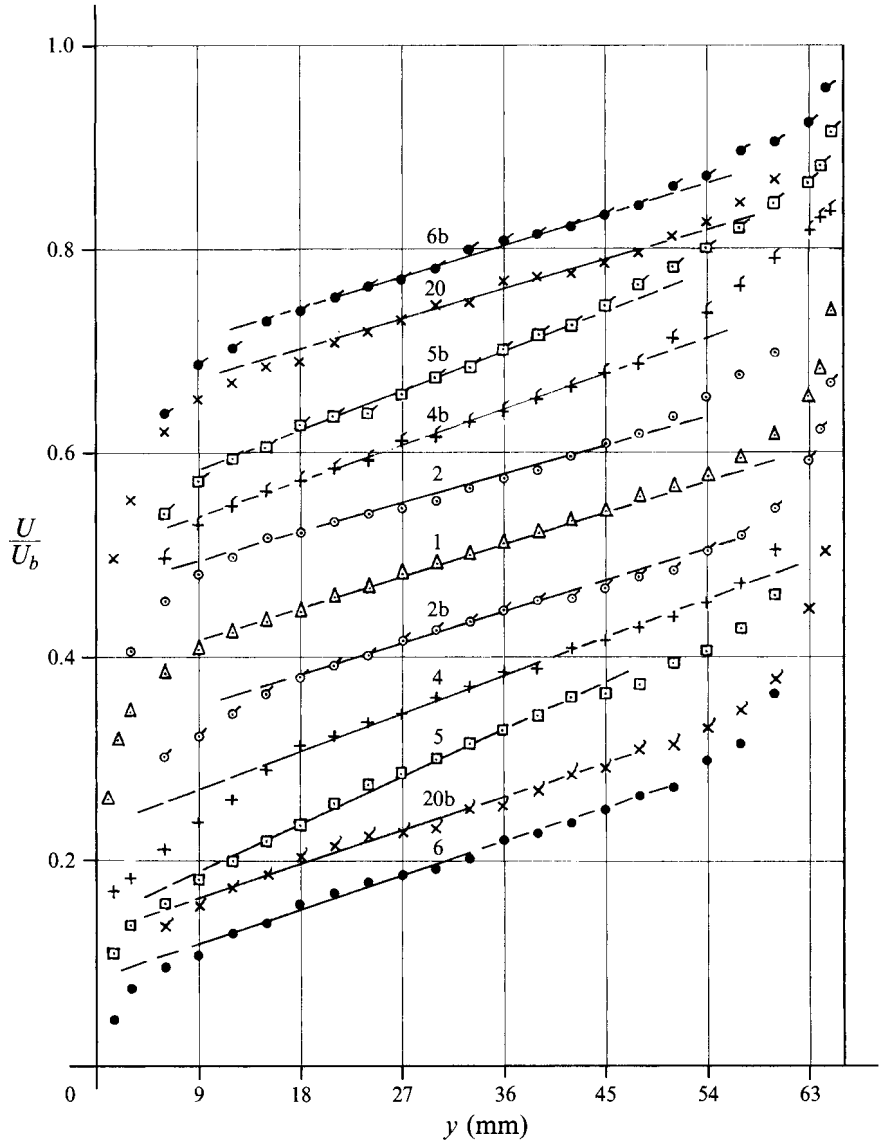

FIGURE 1. Couette-type flows: mean velocity $(U_b - U)$, as seen from the belt, scaled with belt velocity U_b, *vs.* distance y from the wall. For symbols, see table 1.

In this case the Eulerian equation is

$$(U^3)_{yyyy} = 0, \tag{7}$$

which yields the solution

$$U = [\alpha + \beta y + \gamma y^2 + \delta y^3]^{1/3}. \tag{8}$$

In the 'free turbulence' core region, defined by $y_1 \leqslant y \leqslant y_2$, the integral result (4) now reduces to

$$I = \int_{y_1}^{y_2} [(U^3)_{yy}]^2 \, \mathrm{d}y = 4[\gamma^2 y + 3\gamma\delta y^2 + 3\delta^2 y^3]_{y_1}^{y_2} \to \text{minimum}. \tag{9}$$

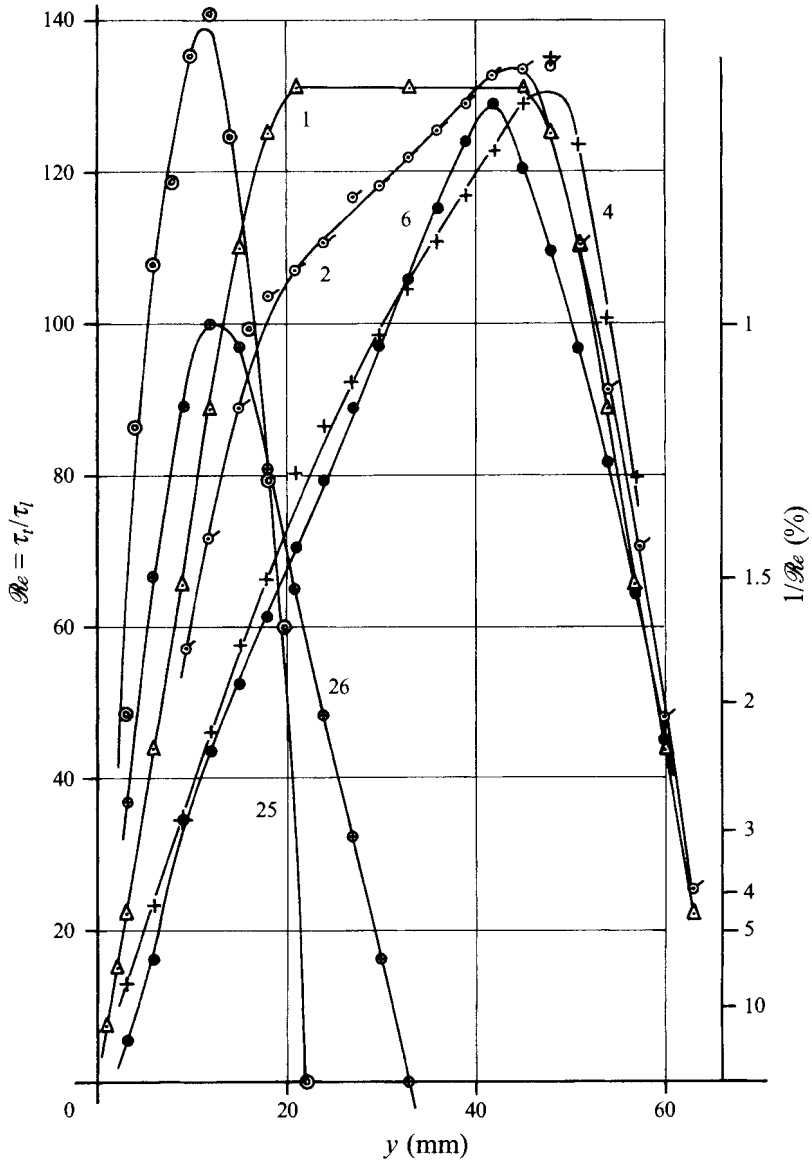

FIGURE 2. Local Reynolds number $\mathscr{R}e = \tau_t/\tau_l$ *vs.* distance y from the wall, for four Couette-type flows (with $2h = 66$ mm) and two pure Poiseuille-type flows (with $2h = 44$ or 66 mm).

In particular, for $\gamma = \delta = 0$ this integral takes on the value zero, and within the core region the relationship between U^3 and y is then given by a straight line.

3. Remarks on unidirectional flows

Some non-dimensionalized Couette-type velocity profiles (U/U_b, with $U_b > 0$ the belt velocity) are shown in figure 1, as seen from the fixed wall or the belt, for various ratios $\lambda = u_{*f}/u_{*b}$ between 0.2 and 5. Here u_{*f} and u_{*b} are the friction velocities defined, respectively, using the wall stress at the fixed wall and the wall stress at the moving wall formed by the belt. Each test case gives two profiles: $U_1(y)/U_b$ and $[U_b - U_2(2h-y)]/U_b$ with $2h$ the channel breadth. A reflection of one profile about the

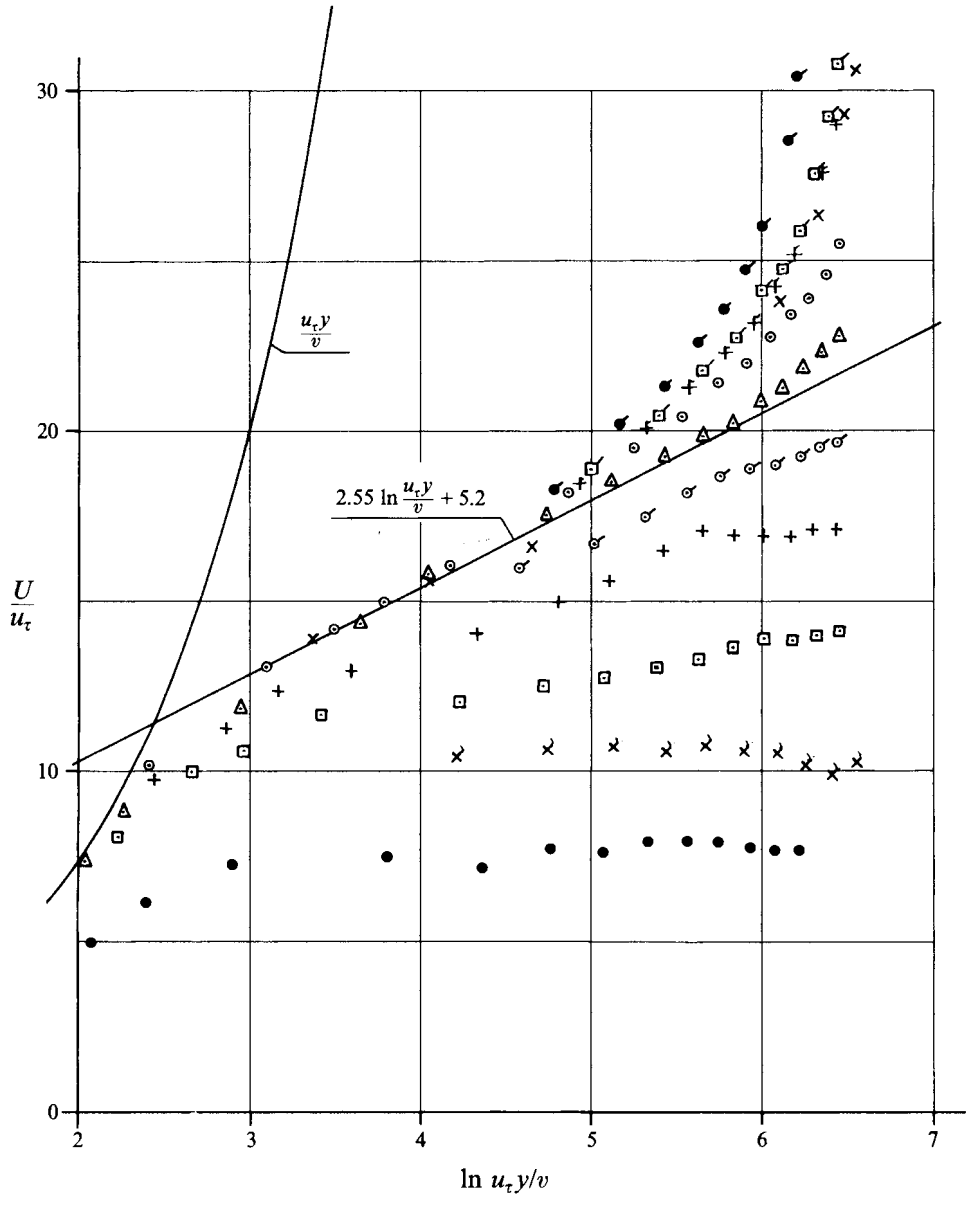

FIGURE 3. Couette-type flows: mean velocity $U(y)$ over local friction velocity $u_\tau(y)$ *vs.* non-dimensional distance $u_\tau y/\nu$, with y measured from the wall or from the moving belt (when it is replaced by $66-y$ mm). Viscosity is taken to be 0.1486 cm^2 s^{-1}. For symbols, see table I.

centreplane $y = h = 33$ mm, followed by a second reflection about $U/U_b = 0.5$, produces the second profile. For example, the highest profile (Case 6, seen from the belt) gives an average velocity $U_{1av} = 6.71$ m s^{-1}, yet the lowest profile (Case 6 measured from the fixed wall) gives the average

$$U_{2av} = U_b - U_{1av} = 8.59 - 6.71 = 1.88 \text{ m s}^{-1}.$$

Hence the conventional Reynolds number can be calculated as either

$$Re_1 = U_{1av} 2h/\nu = 29000 \quad \text{or} \quad Re_2 = U_{2av} 2h/\nu = 8350.$$

To define a flow of this kind, one has to know the belt velocity, and also the shear

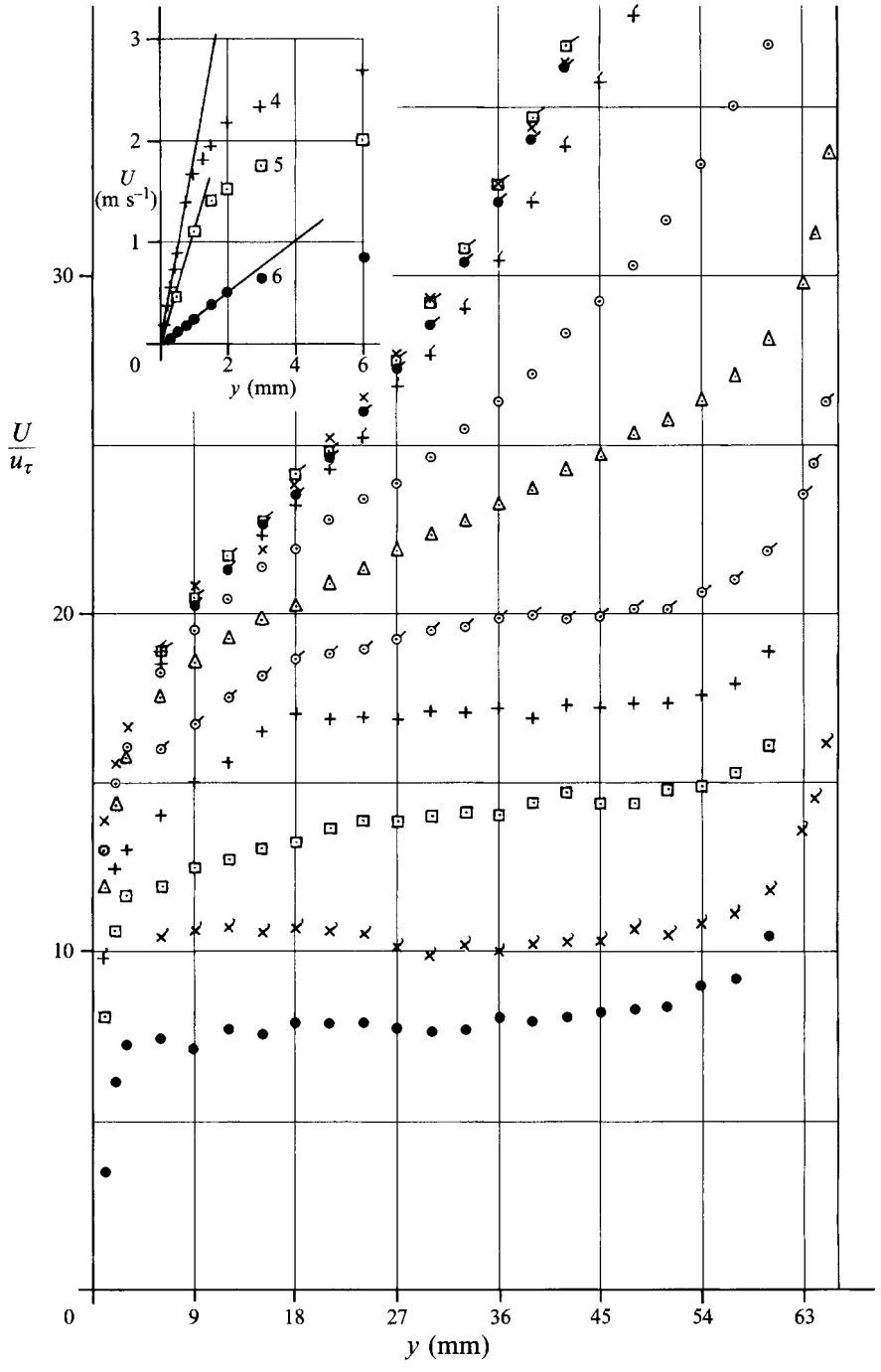

FIGURE 4. Couette-type flow of figure 3: U/u_τ *vs.* distance y and $(U_b - U)/u_\tau$ *vs.* $(66 - y$ mm). In the top left-hand corner are shown three viscous sublayers.

stresses at the fixed and moving walls, u_{*f} and u_{*b} (not merely their ratio) which incorporate the effect of blowing through the channel.

On the other hand, in unidirectional flow the total shear stress is known through the flow, since it varies linearly with the coordinate y measured normal to the flow. We can

Symbol	Case	U_b (m s^{-1})	$\lambda = u_{*0}/u_{*66}$	n	$10^3 \times (\overline{U^n})/U_b^n$	Core region
●	6b	8.50	5.089 (0.313/0.0615)	1	$3.370y+682.2$	$21 \leqslant y \leqslant 45$
				3	$6.339y+291.9$	
				5	$6.643y+98.67$	
×	20	12.84	3.958 (0.431/0.1089)	1	$3.215y+645.0$	$21 \leqslant y \leqslant 45$
				3	$5.415y+246.4$	
				5	$5.077y+74.08$	
□	5b	12.84	2.935 (0.383/0.1305)	1	$4.383y+542.6$	$18 \leqslant y \leqslant 42$
				3	$5.992y+127.5$	
				5	$4.576y+4.449$	
+	4b	12.84	2.142 (0.357/0.1667)	1	$3.920y+501.0$	$21 \leqslant y \leqslant 45$
				3	$4.685y+97.68$	
				5	$3.128y-1.329$	
○	2	12.84	1.408 (0.328/0.233)	1	$3.154y+462.9$	$21 \leqslant y \leqslant 45$
				3	$3.072y+81.92$	
				5	$1.669y+4.623$	
△	1	12.84	1 (0.252/0.252)	1	$3.522y+383.8$	$21 \leqslant y \leqslant 45$
				3	$2.646y+38.70$	
				5	$1.112y-4.522$	
○	2b	12.84	0.710 (0.233/0.328)	1	$3.384y+322.0$	$18 \leqslant y \leqslant 42$
				3	$1.757y+23.99$	
				5	$0.5418y-2.107$	
+	4	12.84	0.467 (0.1667/0.357)	1	$4.106y+2.339$	$15 \leqslant y \leqslant 39$
				3	$1.451y+2.859$	
				5	$0.2907y-2.565$	
□	5	12.84	0.341 (0.1305/0.383)	1	$5.270y+141.3$	$12 \leqslant y \leqslant 36$
				3	$1.124y-6.444$	
				5	$0.1404y-1.675$	
×	20b	12.84	0.253 (0.1089/0.431)	1	$3.258y+140.1$	$12 \leqslant y \leqslant 36$
				3	$0.4596y-0.1981$	
				5	$0.03729y-0.3319$	
●	6	8.59	0.196 (0.0615/0.313)	1	$3.764y+83.29$	$9 \leqslant y \leqslant 33$
				3	$0.2865y-1.322$	
				5	$0.01475y-0.1703$	$15 \leqslant y \leqslant 33$

Notes: (i) Case 20 (×) related to the belt is labelled Case 20 b (×). (ii) u_{*0} is friction velocity at $y = 0$; u_{*66} is at $y = 2h = 66$ mm. (iii) Best-fit lines apply in the core region; see equation (13) for notation.

TABLE 1. Characteristics of Couette-type flows, related to the fixed wall

define a local friction velocity in terms of the local shear stress and relate it to the friction velocities for the two walls:

$$u_\tau^2 = |\tau/\rho| = u_{*f}^2 + (u_{*b}^2 - u_{*f}^2)\frac{y}{2h}, \tag{10}$$

with y measured from the fixed wall. This total stress has laminar and turbulent components:

$$\tau = \rho\nu U_y - \rho\overline{u'v'} = \tau_l + \tau_t \tag{11}$$

and this suggests that a local Reynolds number can be defined as

$$\mathscr{R}e = \frac{\tau_t}{\tau_l} = \frac{\tau - \tau_l}{\tau_l} = \frac{u_\tau^2}{\nu U_y} - 1. \tag{12}$$

Examples of the variation of $\mathscr{R}e(y)$ are given in figure 2. For the Couette-type flows that are considered, the two profiles of each test give the same variation, but reflected

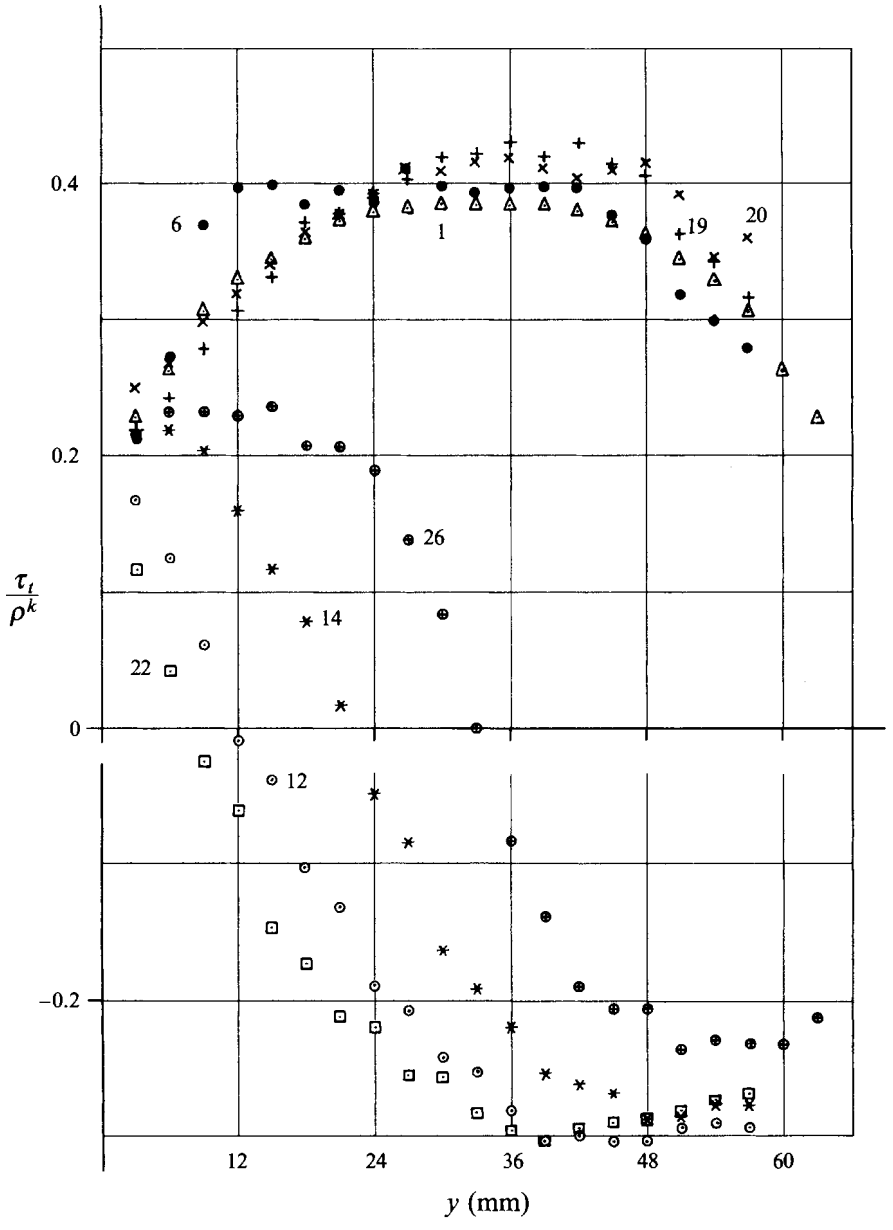

FIGURE 5. Ratio τ_t/k of turbulent mixing stress to turbulence kinetic energy. See table 1 for case numbers.

in the centre plane. The maximum value $\mathscr{R}e_{max}$ is almost the same, close to 130, for the several tests. The reason for this behaviour may be that the average value

$$(u_\tau^2)_{av} = \tfrac{1}{2}(u_{*f}^2 + u_{*b}^2)$$

varies only a little from flow to flow. Note that this average is closely related to the 'effective' friction velocity that was introduced by El Telbany & Reynolds (1981):

$$u_e = (u_{*f}^2 + u_{*b}^2)^{1/2} = (2u_\tau^2)^{1/2}.$$

The average value of $\mathscr{R}e$ depends, of course, on the conventional Reynolds number and on the flow type. Considering, for example, Case 1 of figure 2 (pure Couette flow), we have $\mathscr{R}e_a = 87.5$, while the conventional Reynolds number based on channel half-width h and centreline velocity U_c is $Re_c = U_c h/\nu = 14260$. Thus we obtain $Re_c/\mathscr{R}e_a = 163$. For all four cases of pure Couette flow that have been considered (with $Re = 9500$ to 19000) this ratio is

$$Re_c/\mathscr{R}e_a = 164 \pm 5\%.$$

On the other hand, for pure Poiseuille flow, the ratio is $423 \pm 5\%$.

Since the local value of u_τ is known for the 'simple' flows considered here, one might seek to extend the range of applicability of the law of the wall, for both fixed and moving walls. For Couette-type flows the results are shown in figures 3 and 4, with values of the parameter λ between 5 and 0.2. Further details are given in table 1. It is mainly near the walls (fixed or moving) when $\lambda < 1$ that the modified law of the wall differs from the conventional form, in which the friction velocity is assigned the fixed value pertaining at the adjacent wall. This is because the change in the local friction velocity is much greater in such cases. The velocity profiles of figure 4 also differ much more when $\lambda < 1$ than when $\lambda > 1$, and a core region appears, with U/u_τ virtually constant. However, for the side where $\lambda \geqslant 1$ the conventional law of the wall provides an adequate representation.

The presentation in figure 5 of results given in El Telbany & Reynolds (1981, 1982) may be useful in improving current models of turbulence. It shows the relationship between the turbulent stress ($\tau_t = -\rho\overline{u'v'}$) and the turbulence energy defined as usual by

$$k = \tfrac{1}{2}(\overline{u'^2} + \overline{v'^2} + \overline{w'^2}) \quad \text{per unit volume.}$$

For pure Couette flow, Schneider (1989) has already proposed a more general diffusion mechanism for Reynolds stresses. Note that the distribution obtained is nearly the same for all S-shaped profiles of mean velocity. (The deviation of the points at $y = 9$ to 15 mm in Case 6 may be due to the extremely thick viscous sub-layer shown in figure 4.)

For pure Poiseuille flow and other U-shaped velocity distributions within which the direction of the turbulent stress changes, a considerable variety of distributions is to be seen in figure 5.

4. Couette-type or S-shaped velocity profiles

In any S-shaped curve there must, of course, be a region near the point of inflexion where the curve is nearly linear. However, it is remarkable that in figure 1 all of the plots of U/U_b *vs.* y display quasi-linear regions that extend over nine measured values, and thus indicate a core region whose width is just over one third that of the channel. On the other hand, the simplest solution consistent with the variational principle would be a linear variation of $U^3(y)$, as shown earlier. The plots of figure 6 confirm this prediction as well, for the central part of the channel.

The best linear fit was calculated for each of the profiles $(U/U_b)^n$, for $n = 1, 3$ and 5; the results are given in table 1. To determine the power n giving the best approximation to the test data $U_d(y)$, plots of the form of figures 7(*a*) and 7(*b*) were prepared. These show the ratios (respectively marked by +, ○ and ●)

$$\frac{U_d}{(U^n)^{1/n}} \quad \text{for} \quad n = 1, 3 \text{ and } 5. \tag{13}$$

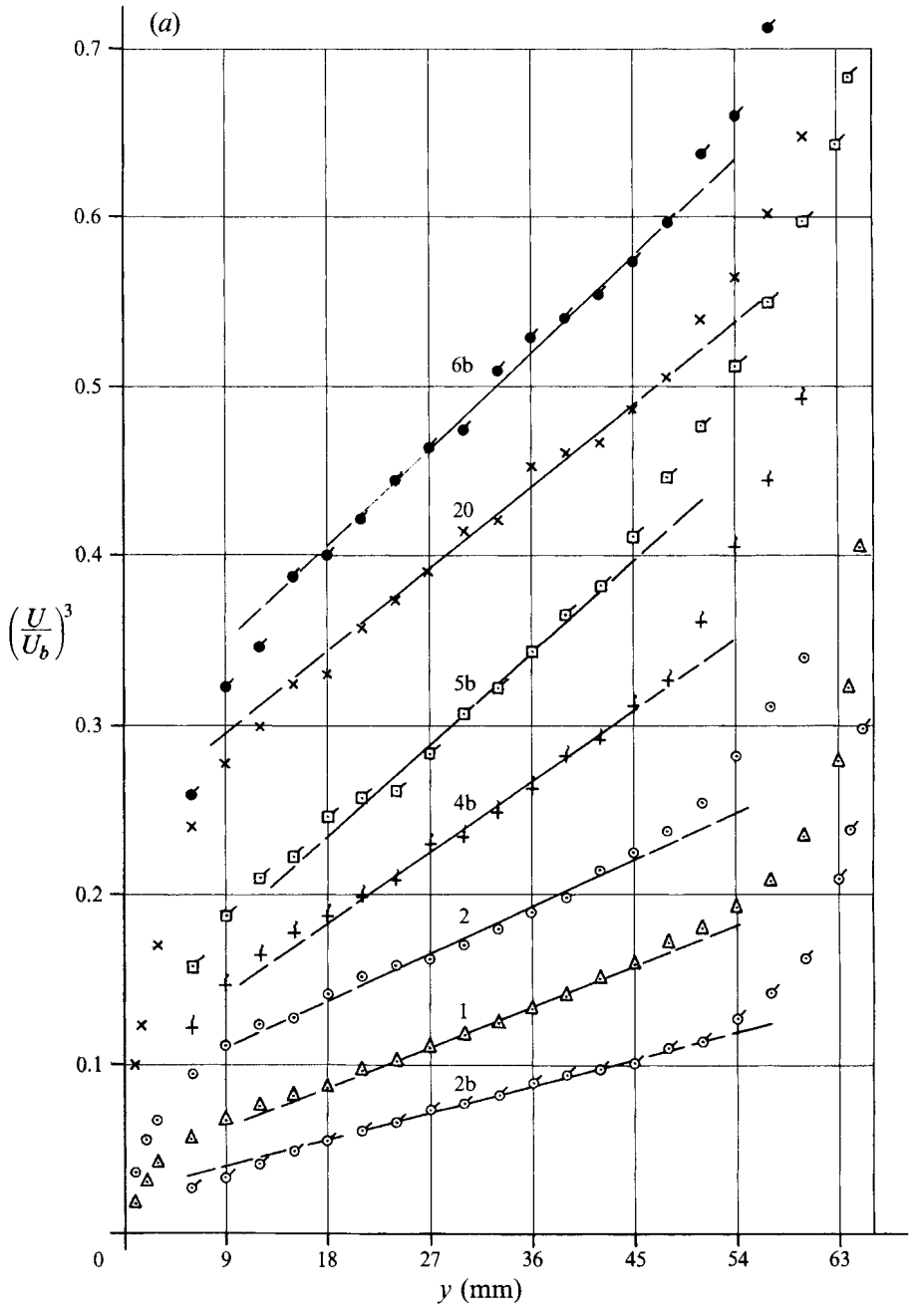

FIGURE 6(*a*). For caption see facing page.

Figure 7(*a*) (which relates to Case 20) shows that the differences among the best-fit results themselves are small, being typically less than 0.1%. The scatter of the data is greater, however, although it is here less than 1%. The curve that is shown gives the ratio $\bar{U}/(U^3)^{1/3}$. Only at the edge of the core region do the best-fit values differ by as much as 0.15%.

Figure 7(*b*) also presents data relating to Case 20, but now as seen from the belt. In this extreme example the velocities are only one-quarter to one-third of those measured

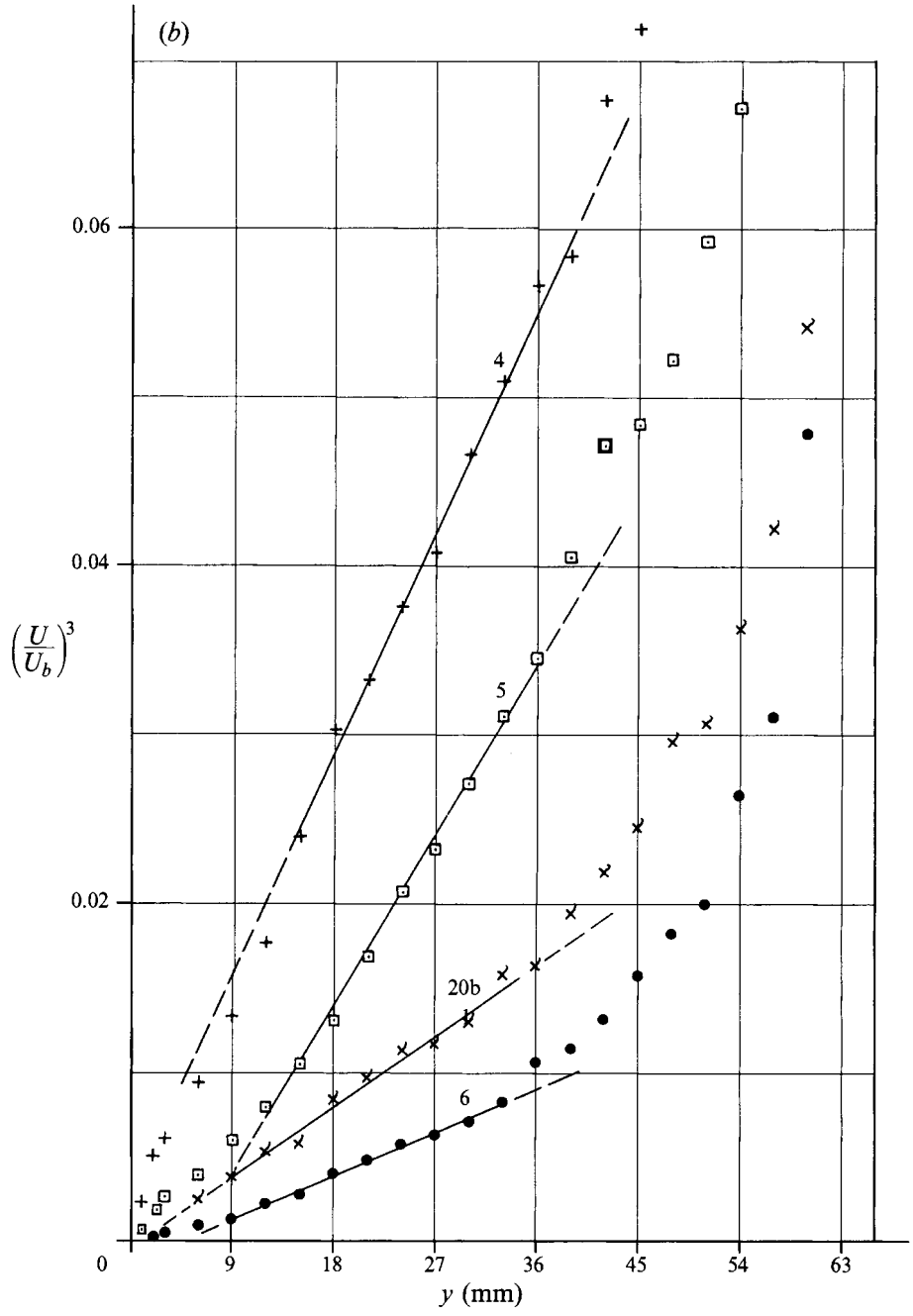

FIGURE 6. Profiles of velocities raised to the third power for the cases considered in figure 1, displaying a linear core region. For symbols, see table 1.

from the fixed wall. Accordingly, the experimental scatter is now about 3%, and again greatly exceeds the differences between the best-fit results.

We see that the scatter in the test values is sometimes in excess of 2%, while the best-fit approximations generally deviate from one another by less than 1%. These differences between best-fit approximations could be made even smaller by reducing

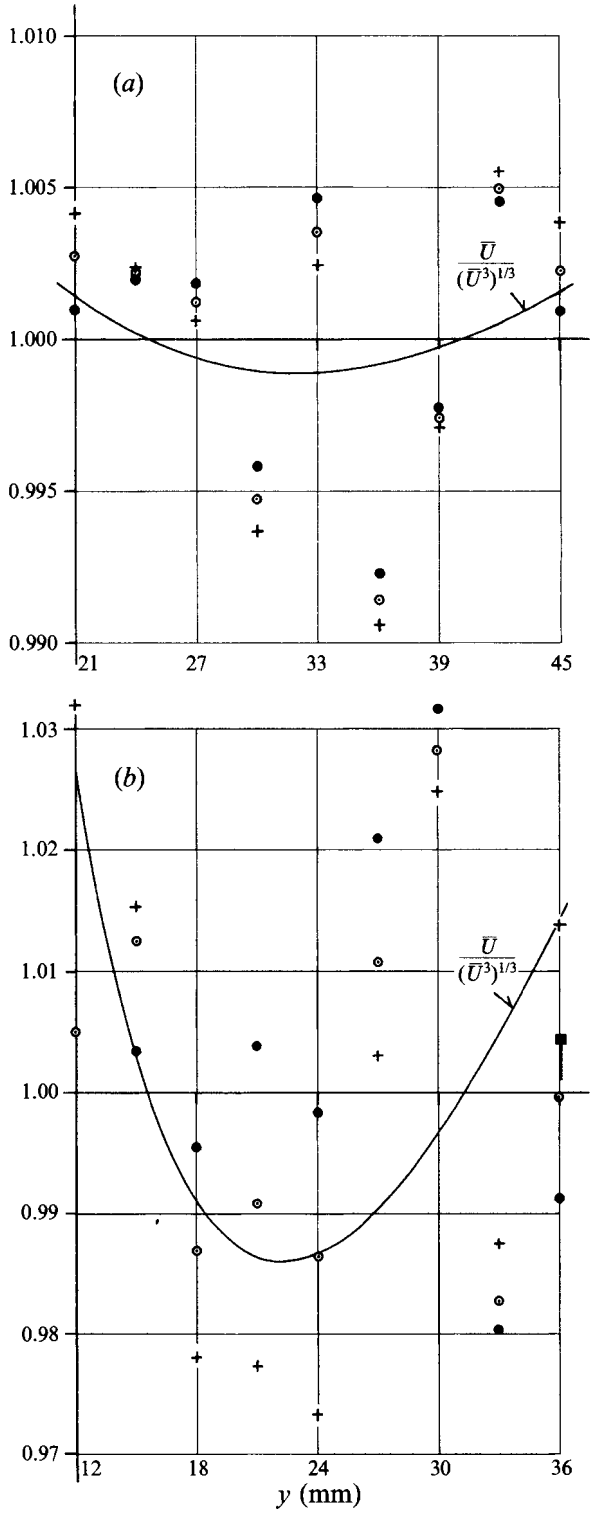

FIGURE 7. Comparison of best linear fits of the quantities defined in equation (13) *vs.* distance y for $n = 1, 3, 5$ (+, ⊙, ● respectively): test data of Case 20 for the core region. (*a*) Seen from the fixed wall; (*b*) seen from the moving belt.

y	U_d	$\bar{U}/U_d$	$(\overline{U^3})^{1/3}/U_d$	$(\overline{U^5})^{1/5}/U_d$
6	6.73	1.0783	1.0565	1.0214
9	7.10	1.0423	1.0279	1.0061
12	7.31	1.0319	1.0228	1.0106
15	7.58	1.0140	1.0089	1.0024
18	7.80	1.0037	1.0013	0.9985
21	7.97	1.0003	0.9996	0.9989
24	8.11	1.0006	1.0010	1.0013
27	8.27	0.9986	0.9992	0.9997
30	8.40	1.0001	1.0004	1.0007
33	8.54	1.0005	0.9999	0.9994

TABLE 2. Best-fit results for pure Couette flow (Case 18) for core region $21 \leqslant y \leqslant 33$ mm

the posited breadth of the core region. Hence it is quite impossible to decide whether test data in the core region are better approximated by the simple linear variation or by the cubic velocity variation indicated by the variational principle.

5. Pure Couette flow

Because of the theoretical importance of pure Couette flow, details will be given for Case 18, which is that with the highest Reynolds number, $Re_c = U_c h/\nu = 18960$, and with $h = 33$ mm, $U_c = \frac{1}{2}U_b = 8.54$ m s^{-1}, $u_{*f} = u_{*b} = 0.363$ m s^{-1}. For the core region, $21 \leqslant y \leqslant 33$ mm, the best linear fits of the test data (measured relative to the fixed wall) are

$$\overline{U_d} = 6.971 + 0.04767y,$$
$$\overline{U_d^3} = 301 + 9.748y,$$
$$\overline{U_d^5} = 8691 + 1109y.$$

In table 2 these results are compared with test data. The comparison shows that the variations $\overline{U_d^3}$ and $\overline{U_d^5}$ go some way towards providing a smooth transition of the complete profile $U(y)$ from the nearly linear core region to the logarithmic law of the wall. Still, in the core region itself, the formulae differ so little that it is hardly possible to prefer one to another.

On the other hand, test results such as are considered here are usually presented, as in figure 8, in the form of plots of $(U_c - U)/u_*$ *vs.* $(1 - y/h)$. To do this, the best-fit constants for the law of the wall were first determined for each test case, and thence the tangent of the law of the wall that leads to the zero of velocity at the wall. Obviously, this approximation is also quite adequate, for the accuracy of these measurements. Table 3 gives numerical details.

6. Poiseuille-type or U-shaped velocity profiles

When the belt moves in the direction opposite to blowing, there will exist an extreme value of velocity within the channel, either a maximum or minimum, depending on the coordinate system chosen. In the region of this extreme value we cannot expect to find a linear distribution of $U^3(y)$, corresponding to $I = 0$ for the region.

Consider two points, one on each of the logarithmic distributions that describe the velocity variations near the walls, at which the velocities are identical and at which the tangents are identical to those of the corresponding laws of the wall (or, in the situation

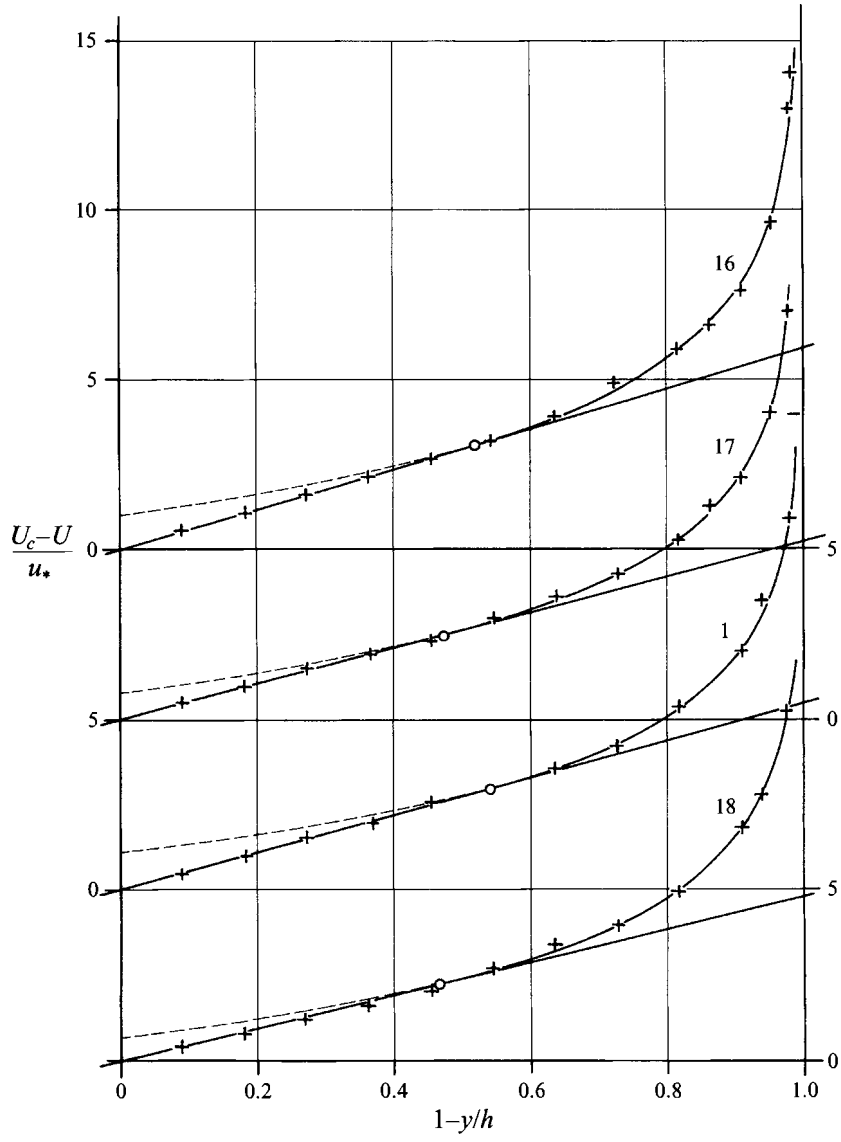

FIGURE 8. Another plot of the four cases of pure Couette flow: U_c = centreplane velocity at $y = h$ = half-channel width. u_τ is the constant friction velocity (see table 3).

Case	h (mm)	U_c (m s^{-1})	$U_c h/\nu$	u^* (m s^{-1})	κ	C
16	22	6.42	9500	0.293	0.35	3.62
17	22	4.27	12640	0.378	0.37	4.62
1	33	3.21	14260	0.282	0.40	5.65
18	33	4.27	18960	0.363	0.38	5.46

TABLE 3. Details of pure Couette flows of figure 8

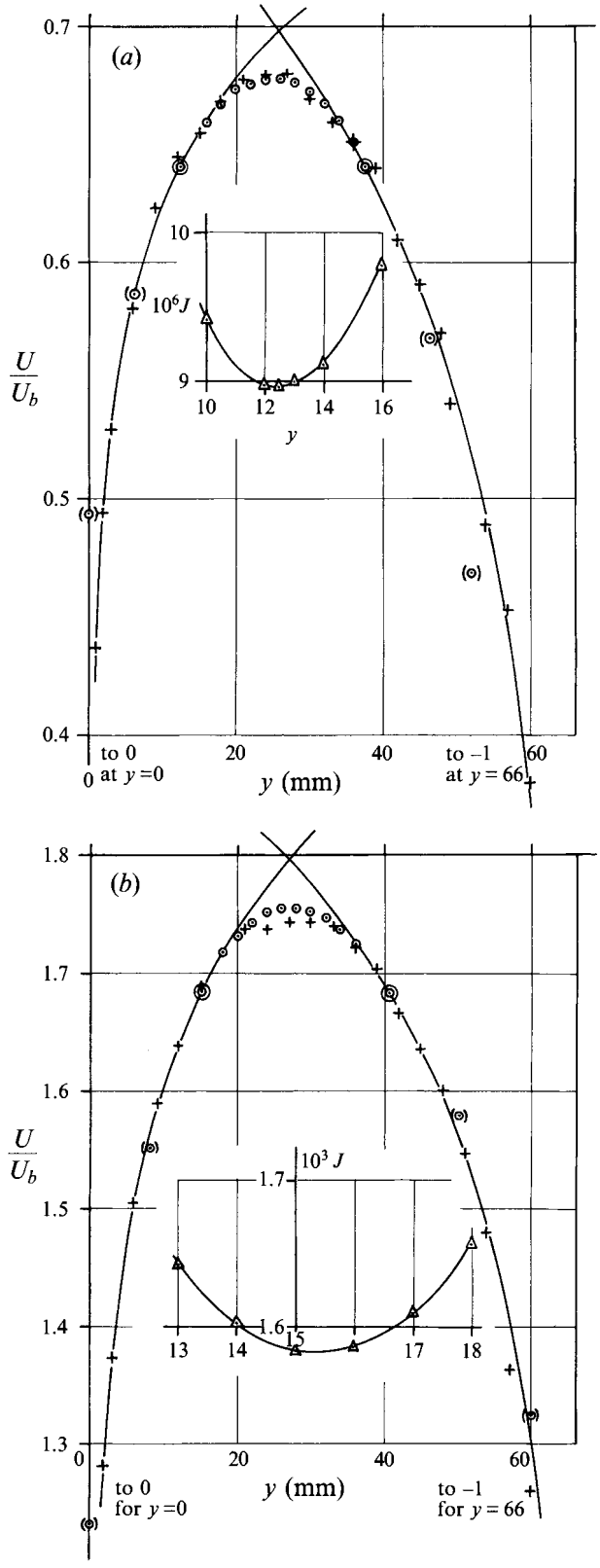

FIGURE 9. Velocity profiles for the reversed flow of (*a*) Case 12 and (*b*) Case 14: + test points; ⊙ solution for which the integral I of equation (9) is a minimum.

For figure 9(*a*), Case 12

$$\frac{U}{U_b} = \frac{0.4142}{12.84}\left[2.39\ln\left(4.142\frac{y}{\nu}\right)+5.9\right] \quad \text{at the fixed wall}$$

$$\frac{U}{U_b} = \frac{0.88}{12.84}\left[2.48\ln\left(\frac{8.8(66-y)}{\nu}\right)+5.55\right]-1 \quad \text{at the belt}$$

$$U/U_b = [\alpha+\beta y+\gamma y^2+\delta y^3)^{1/3} \quad \text{in the core flow}$$

with $\alpha = 0.1203, \quad \beta = 0.01546, \quad \gamma = -3.203\times10^{-4}, \quad \delta = 3.170\times10^{-7}$

For figure 9(*b*), Case 14

$$\frac{U}{U_b} = \frac{0.67}{8.59}\left[2.49\ln\left(6.7\frac{y}{\nu}\right)+5.35\right] \quad \text{at the fixed wall}$$

$$\frac{U}{U_b} = \frac{0.961}{8.59}\left[2.35\ln\left(\frac{9.61(66-y)}{\nu}\right)+6.6\right]-1 \quad \text{at the belt}$$

$$U/U_b = [\alpha+\beta y+\gamma y^2+\delta y^3]^{1/3} \quad \text{in the core flow}$$

with $\alpha = 1.861, \quad \beta = 0.2846, \quad \gamma = -6.541\times10^{-3}, \quad \delta = 3.125\times10^{-5}$

TABLE 4. Details for figures 9(*a*) and 9(*b*) ($\nu = 0.1485$ cm^2 s^{-1}; y in mm)

considered here, the belt). For any two such points it is possible to find the four constants of equation (8) and thus to determine a smooth transition between the two wall layers. However, the choice which makes the integral I a minimum gives a velocity profile in the core region that deviates very little from the test data. Two comparisons of measurements with profiles calculated in this way are shown in figures 9(*a*) and 9(*b*). The absolute values of the modelled and measured velocities differ by less than 1%. The inset figures show how the maximum deviation depends on the location of the matching point.

It is remarkable how closely the calculated polynomials (points marked ⊙) follow the wall laws even outside the core region. For details, see table 4.

7. Pure Poiseuille flow

For these cases – with the belt at rest – test accuracy is very high, say within 0.5%. However, there is again a region where $U(y)$ and $U^3(y)$ are both essentially linear, so that $I = 0$ over the region. Figure 10 illustrates the fitting of the latter variation to two of these velocity variations. It should be realized that in this form of plot an uncertainty in U of 0.5% becomes one of 1.5%; this is illustrated for three points.

Using also the logarithmic variations near the walls, we are able to describe the velocity profile almost completely. Only very near the centre of the channel does the velocity profile revert to a parabola, for which $I > 0$. Further measurements, preferably at higher Reynolds numbers, would provide here a more conclusive test of the principle.

8. Concluding remarks

A variational principle relating to the profile of mean velocity in free-turbulent flow has been confirmed using data describing a variety of unidirectional channel flows of Couette and Poiseuille types. This is, admittedly, only a mathematical experiment, since an intuitive or physically based explanation cannot be offered to support the

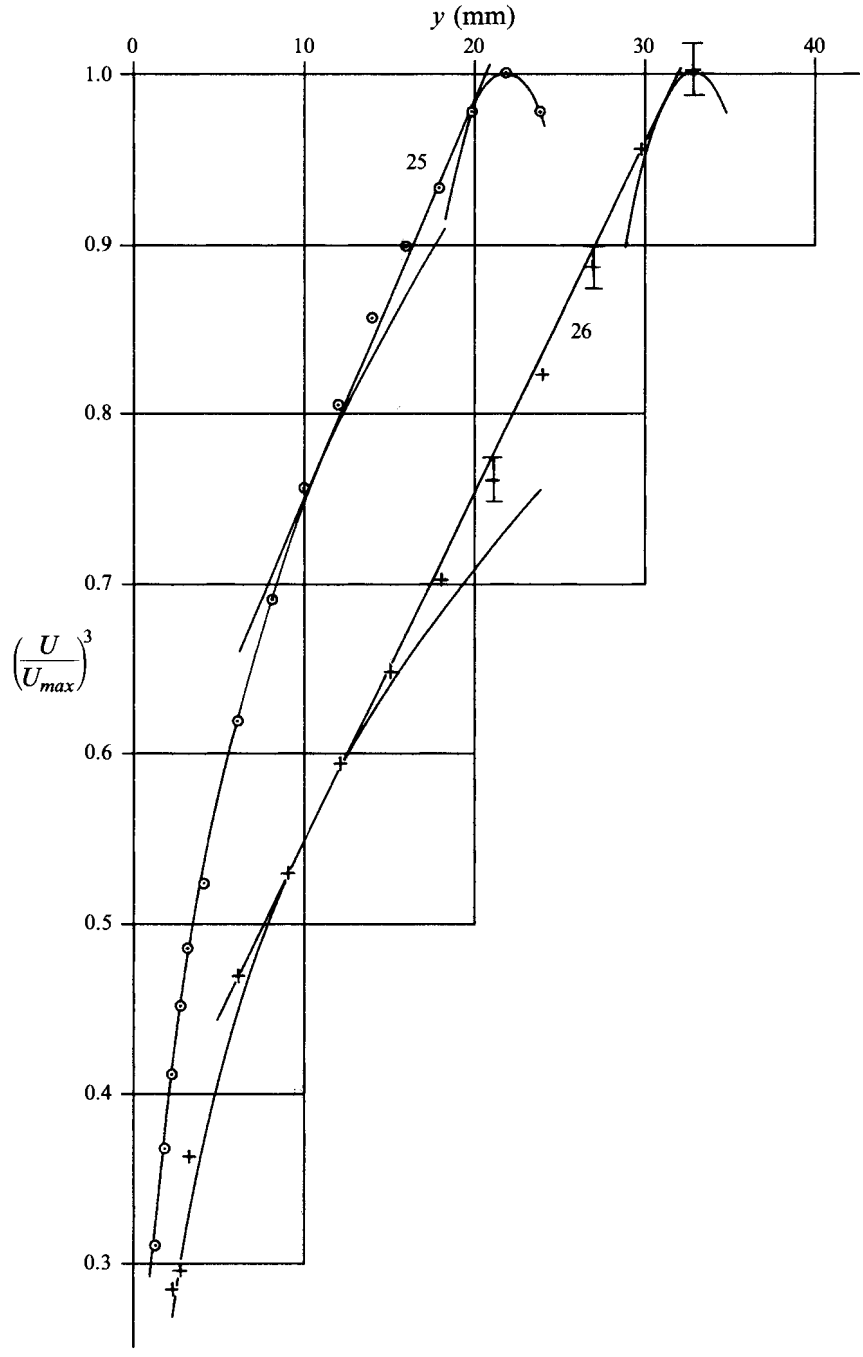

FIGURE 10. Profiles of velocity raised to the third power: pure Poiseuille flow, Cases 25 and 26.

findings. However, the model derived from the variational principle has earlier been found to provide adequate representations of significant parts of the velocity variations in tube flow, in two-dimensional boundary layers, and in free jets.

It is of interest to note another attempt to use a variational principle to determine flows subject to friction forces. Helmholtz (1868) introduced an intuitively very

attractive principle of minimum dissipation, for creeping flow at very small Reynolds number. For this case the Navier–Stokes equation reduces to

$$\nu \operatorname{rot} \operatorname{rot} \bar{V} = -\frac{\nabla p}{\rho}.$$

Later, Lord Rayleigh (1913) remarked that this principle would be valid for any Reynolds number, provided only that the friction stress can be expressed as a potential function, P, say, that is, when $\operatorname{rot}^{III} V = 0$. It is obvious that this condition is satisfied when P = constant or when P is a linear function of the spatial coordinates, as is the case in Poiseuille flow. However, it has been shown (Görtler & Wieghardt 1942), for two-dimensional flows at least, that in this case no further exact solution of the Navier–Stokes equations exists.

REFERENCES

Coles, D. E. & Hirst, E. A. (Eds) 1968 *Proc. Computation of Turbulent Boundary Layers*, Vol. II. Stanford University.

El Telbany, M. M. M. & Reynolds, A. J. 1980 Velocity distributions in turbulent channel flows. *J. Fluid Mech.* **100**, 1–29.

El Telbany, M. M. M. & Reynolds, A. J. 1981 Turbulence in plane channel flows. *J. Fluid Mech.* **111**, 283–318.

El Telbany, M. M. M. & Reynolds, A. J. 1982 The empirical description of turbulent channel flows. *Intl J. Heat Mass Transfer* **25**, 77–86.

Görtler, H. & Wieghardt, K. 1942 Über eine gewisse Klasse von Strömungen zäher Flüssigkeiten und eine Kennzeichnung der Poiseuille-Strömung. *Math. Z.* **48**, 247.

Helmholtz, H. 1868 Zur Theorie der stationären Ströme in reibenden Flüssigkeiten. Verh. des naturhist.-med. Vereins.

Knaack, Th. 1992 Untersuchungen der Struktur des Reynolds-Tensorfeldes in einer dreidimensionalen Strömung. Diss. Hamburg, Inst. für Schiffbau, Bericht 527.

Rayleigh, Lord 1913 On the motion of a viscous fluid. *Phil. Mag.* **XXVI**, 776.

Schneider, W. 1989 On modelling the transport of turbulent kinetic energy in Couette Flow. *Z. Angew. Math. Mech.* **69**, 627–629.

Wieghardt, K. 1990 On a characteristic of three-dimensional free turbulence. *12th Georg Weinblum Memorial Lecture, Schiffstechnik 37, Sonderdruck*, pp. 35–46.

Wieghardt, K. 1991 Zum Aussengesetz inkompressibler, turbulenter Grenzschichten. *Z. Flugwiss. Weltraumforsch.* **15**, 319–322.